TOWARDS HIGH-PRECISION CONTROL OF TRANSFORMATION CHARACTERISTIC IN VO2 THROUGH DOPANT MODULATION OF HYSTERESIS

A Thesis

by

ALIYA JANAE YANO

Submitted to the Office of Graduate and Professional Studies of
Texas A&M University
in partial fulfillment of the requirements for the degree of

MASTER OF SCIENCE

Chair of Committee,	Patrick Shamberger
Committee Members,	Sarbajit Banerjee
	Kelvin Xie
Head of Department,	Ibrahim Karaman

May 2021

Major Subject: Material Science and Engineering.

ABSTRACT

As we approach the limits of what traditional computer architecture is capable of, a new system is needed to continue growth in computational power. One solution lies in neuromorphic systems and, specifically, those that utilize specialized materials capable of inherently mimicking brain functions. Due to its metal-insulator transition (MIT) at ~68C and the accompanying magnitude change in electronic resistance, VO2 is one such material. Previous studies have shown that the transition temperature can be tuned through chemical doping, but little is known about how these dopants affect the microscopic progression of the phase transformation through a volume. This is critical as changes to the MIT directly affect the functionality of VO2 in these devices and could enable control over various aspects of the transition such as degree of volatility. Therefore, a more mechanistic understanding of how dopants affect transformation behavior is needed. Here we utilize an optical technique to investigate the effects of substitutional tungsten, and interstitial boron dopants on the MIT behavior in VO2 compared to its undoped state. Tungsten demonstrates the ability to depress the transition temperature, reduce hysteresis and increase the width of transformation. Boron also induces a small increase in transformation width but maintains a hysteresis similar to undoped while exhibiting unique relaxation behavior. In addition, both dopants negate size effects observed in undoped particles. Likely due to their ability to enhance or suppress point defect concentrations and thereby improve the consistency of hysteresis. Both effects are vital for practical application of VO2 in neuromorphic devices which require precise control of transformation characteristics.

ACKNOWLEDGEMENTS

I would like to thank my committee chair, Dr. Shamberger and my committee members, Dr. Banerjee and Dr. Xie for their continued patience, guidance and support throughout the course of this research.

Also, a giant thanks to my family and friends for their encouragement and unconditional love.

CONTRIBUTORS AND FUNDING SOURCES

Contributors

This work was supervised by a thesis committee consisting of Dr. Shamberger and Dr. Xie of the Department of Material Science and Dr. Banerjee of the Department of Chemistry.

All samples used in this work were provided by Dr. Banerjee and his team in the Department of Chemistry.

Funding Sources

Graduate study was supported by a fellowship from Texas A&M University and the Data-Enabled Discovery and Design of Energy Materials (D3EM) program funded through NSF award #1545403.

This work was also made possible in part by the President's Excellence Fund, TAMU X-Grants program, NSF award #1545403 and from the Welch Foundation by award #A-1978-20190330. Its contents are solely the responsibility of the authors and do not necessarily represent the official views of any supporting organizations.

TABLE OF CONTENTS

Page

TABLE OF FIGURES

CHAPTER 1

INTRODUCTION AND LITERATURE REVIEW

1.1 Motivation

The last half century has been defined by the rise of the computer. Each year newer and smaller devices are created, every iteration with more computational ability and greater data storage. These advances were enabled by the invention of the transistor in 1947 which incited a need for the development of silicone-based technology and traditional computer architectures. Since it's invention, the transistor has been rapidly decreasing in size from year to year. Allowing for denser circuitry that incorporates billions of transistors in a single chip[1]. However, this rate of exponential advancement is expected to reach a plateau—coming head to head with the laws of physics—as improvements to transistors slow[2]. This trend was predicted in 1965 by Gordon Moore, who anticipated that the success of conventional transistor-based architectures would eventually come to a standstill[3]. With this prediction playing out in the near future, researchers are looking towards alternative architectures for computation and data storage to continue progressing the field.

One such alternative is found in biology-inspired neuromorphic architectures. Though initially developed in the 1980s, neuromorphic architecture only recently became the subject of much interest and has experienced a surge in research and development. These systems are modeled after our own brains, with functions designed

to mimic aspects of neurons and synapses and the potential to be more energy efficient while also enabling advanced computation[4]. Currently, functioning neuromorphic devices exist but require hundreds of elements to emulate simple neurological behavior and lack much of the dynamic and stochastic aspects of neuron networks[5, 6]. There has therefore been a drive to develop new circuit elements out of materials with properties that can inherently lend themselves to mimicking neurological behavior. Memristive materials are the most promising due to the pinched hysteresis seen in a region of their current-voltage profile[5, 7]. Architecture utilizing elements of memristive materials would also be more efficient in use of space and energy than any current neuromorphic devices[5, 6]. However, fundamental understanding of many of these memristive materials is still lacking and requires further investigation to fully utilize their potential.

1.1 MIT/VO2 background

Metal-insulator transition (MIT) materials, such as niobium dioxide (NbO2) and vanadium dioxide (VO_2), exhibit great potential as memristive elements within neuromorphic circuits. MIT materials are characterized by a solid-to-solid phase transition from insulating to conductive. The transition is often induced by temperature but can be triggered through other input such as strain or current. VO_2 in particular demonstrates a coupled electronic-structural transformation when heated to its critical temperature (TMIT) of ~68C[8]. While NbO_2 and VO_2 are both promising memristive materials and NbO2 has been studied extensively, VO_2 is shown to have more desirable properties for device-based applications. NbO_2 has a TMIT at ~700C and therefore requires temperatures above common operating temperatures[4]. The high TMIT also

means it would be less energy efficient and slower switching. VO_2 will therefore be the focus of this study. At its TMIT VO_2 transitions from an insulating, monoclinic (M1) phase of space group $P2_1/c$ to its metallic, high symmetry rutile phase (R) with space group ($P4_2/mnm$)[8]. This transition results in significant changes to properties, such as a four order of magnitude increase in electrical conductivity[9, 10], nearly one order of magnitude decrease in infrared transmittance[11, 12], and a 60% increase in thermal conductivity[13, 14]. Due to VO_2's strongly correlated electron-phonon interacts, the origins of the MIT is difficult to determine and subject to much debate[8]. Prevailing theories tout a combination of Peierls and Mott-Hubbard transitions[9, 15]. The Peierls theory is based on structural changes where, upon transitions from R to M1, the V-V bonds dimerize and the resulting tilt along the c-axis splits the d// states and upshift the pi* bands inducing a bandgap opening[15-18]. Mott transitions place more emphasis on electron correlation in addition to the structural component. This theory agrees that a structural change causes bands to shift, but also postulates that this is accompanied by a depopulation of the pi* bands and less electron screening in the d// band. The subsequently lower density of free electrons in the d// band then causes it to split and triggers the transition[9, 15].

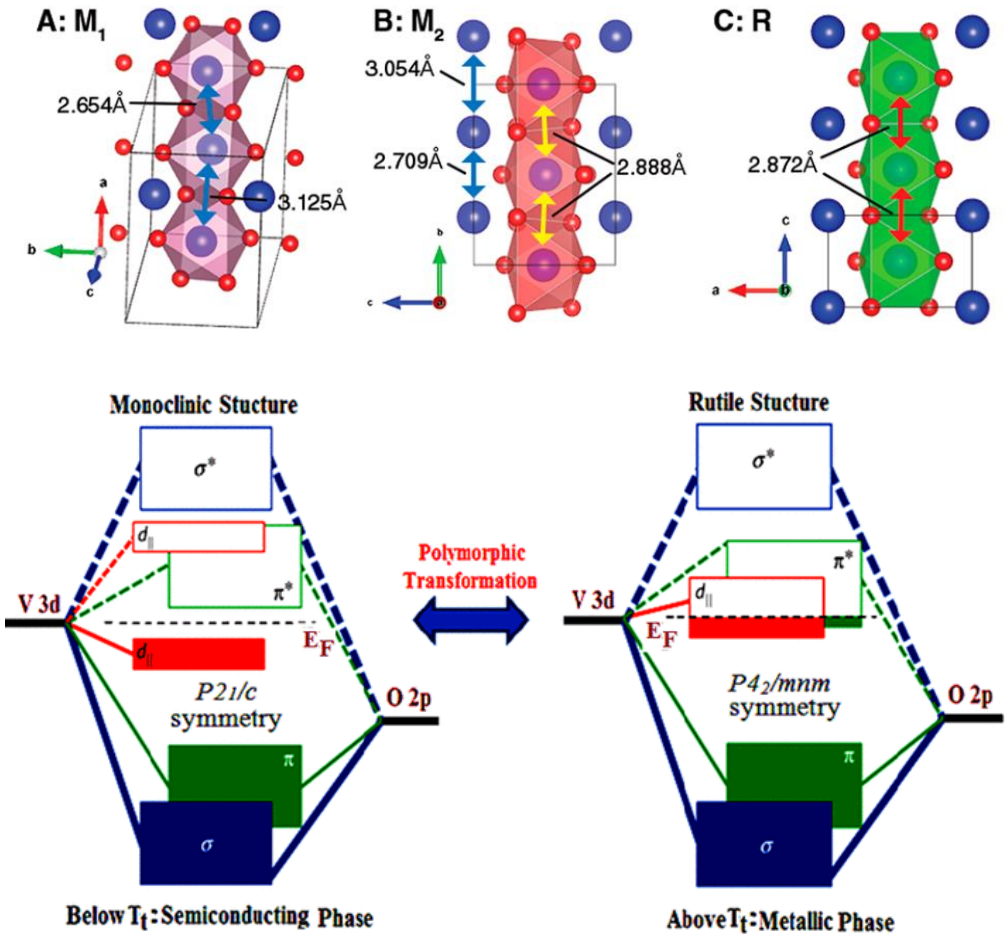

Figure 1: Crystal structures of VO2 in its (A) M1, (B) M2, and (C) R phases[19] and associated bandgaps of the M1 and R phases[20]

VO_2 is regularly studied as freestanding particles, often grown through a hydrothermal process, or as elastically clamped films or particles grown directly onto a substrate[21]. The synthesis method and form of VO_2 can drastically change its transformation behavior since it directly effects the residual stress state of the sample. Elastically clamped VO_2 is known to exhibit a large amount of phase coexistence due to transformation-inducing local strain[22]. In contrast, freestanding, single-crystalline

particles undergo rapid transformation with little phase coexistence. The limited phase coexistence is likely caused by a freestanding particle's ability to deform easily and have limited extended defects that would impede domain growth[23]. Freestanding particles likely use different defects to nucleate phases upon heating and cooling[23, 24]. Stress state of the sample is also important, as it has been shown that an additional monoclinic phase (M2) of space group C2/m forms in both freestanding and elastically clamped particles in the presence of strain [25, 26] whether the strain is mechanical or cause by defects as seen in W-doped particles[27].

1.1.10 Engineering through dopants

More direct control over the transformation behavior is garnered through the careful incorporation of dopants. Slight deviations of the host lattice and electronic structure can have large consequences and the dopants are also able to act as alternative nucleation sites. Dopants can introduce anisotropic strain in the lattice and cause variations of the band structure and, therefore, the Mott behavior[28]. Size and valency of the dopants both play a role in their effects on VO_2, but it is difficult to uncouple their effects and therefore unclear which, if either, is dominant. Numerous studies have been conducted on various dopants to determine effects of dopants on transition behavior. Germanium (+4)[29] and titanium (+4)[30, 31], for example, are two substitutional dopants known to increase the critical temperature of VO_2, while molybdenum (+5)[32] and tungsten (+6)[33] cause significant decreases. Interstitial dopants such as hydrogen or boron have also been incorporated into the VO_2 system, producing unique effects[34, 35]. In general, interstitial dopants are much smaller than their substitutional counterparts which

must be of comparable size to the host lattice[34, 36, 37]. While hydrogen has a very small atomic radius and sit in interstitial tetrahedral sites[34] in the VO_2 lattice, it can have a large impact on the host material: a fully hydrogenated sample exhibits a 13% increase in volume and no longer has an MIT. The disappearance of the MIT at high concentration is thought to stem from the hydrogen interfering with the Peierls transition by impeding the V-V bonds dimerization and the Mott transition by increasing d-orbital occupancy. In this way, increased hydrogen doping preferentially stabilizes the metallic rutile phase by making Peierls and Mott behavior unfavorable— erasing the MIT entirely[28]. Boron is also known to preferentially stabilize the metallic phase but accomplishes this by modifying the phase equilibrium temperature (decreasing critical temperature by ca. 10 °C/atom %)[34] rather than increasing metallicity in the insulating phase and eradicating the MIT, even in highly doped samples. Due to its small size, boron is also highly mobile within the VO_2 lattice which results in unique, time dependent behavior. As the VO_2 host lattice quickly switches between R and M1 phases, the boron is trapped in a metastable site from wherein it relaxes back into its M1 site given enough time[38].

1.1.11 Microscopic Characterization

In the pursuit of better understanding domain nucleation and growth in thin films and freestanding particles, it is necessary to employ various microscopic characterization methods that take advantage of different aspects of the phase change such as differences in optical or electrical properties. For example, a technique utilizing x-ray holography is capable of resolving domains in VO_2 thin films that are at least 50 nm in diameter and

has shown that metallic domains nucleate at and span between nanoscale defects at grain boundaries[22]. This method, employing fine temperature resolution, was able to identify the evolution of individual phases of M1, M2 and R through the transformation. For atomic level measurements, a TEM can be used to monitor transitions as exhibited by Asayesh-Ardakani et al. who monitored the transformation of highly W-doped (0.8 at. % W) single-crystal nanowires in situ[27]. Through this method they were able to corroborate the presence of all three phases (M1, M2, and R) of VO_2 over the transition in samples without epitaxial strain caused by lattice effects [27, 39]. Of course, there are numerous techniques capable of observing microscopic domain evolution; AFM, Raman, and s-SNOM to name a few. However, these methods are known to be expensive spatially and temporally. An alternative technique takes advantage of the change in reflectance seen in the VO_2 transition from M1 to R and tracks these changes optically. While this is more efficient temporally, it also provides a lower resolution. This method was verified by Clarke et al. who used it to collect transformation data such as critical temperature, hysteresis and width of the transformation on an ensemble of ~300 undoped, freestanding VO_2 particles[23]. Clarke et al. was also able to determine that particle size is an important factor in transformation behavior of undoped particles. With increasing particle size, hysteresis was seen to decrease. This is likely due to the number of available nucleation sites, since, statistically, the number of these sites would increase in larger particles. It was also seen that the critical temperature on heating and cooling were uncorrelated. This suggests that the transformation utilizes different nucleation point in each direction[23].

CHAPTER 2

METHODS*

2.1 Synthesis of Doped and Undoped VO_2

Undoped VO_2 particles were hydrothermally synthesized from bulk V_2O_5 powder supplied by Beantown Chemicals, anhydrous oxalic acid ($H_2C_2O_4$) as a reducing agent, acetone/isopropanol, and 2-Allyl-4,4,5,5-tetramethyl-1,3,2-dioxaborolane (97%) from Sigma Aldrich. These particles were prepared with 1.63 g V_2O_5, 10mL of isopropanol and 65 mL deionized water and placed in 125 mL polytetrafluoroethylene cups and heated in a high-pressure autoclave reactor at 210°C for 72 hours. The undoped particles were then recovered through vacuum filtration and washed with deionized water and acetone three times before undergoing a final annealing step at 550°C for 5 hours in an Ar (g) environment in order to relive any strain that may be created during synthesis.

W-doped particles were synthesis through a very similar method, starting with the same precursors and additionally tungstic acid (H_2WO_4) to incorporate the dopant. These samples were made with 300 mg V_2O_5, 450 mg of $H_2C_2O_4$ and the appropriate amount of dopant precursor to obtain desired concentration which was them mixed with 15 mL deionized water. The W-doped mixture was then placed in 23 mL polytetrafluoroethylene cups and heated in the high-pressure autoclave reactor at 250°C for 72 hours. The samples were recovered and placed through the same final annealing step as the undoped particles.

Boron dopants were incorporated in a post-synthesis process by dispersing 20 mg of undoped VO_2 particles in 1.00 mL of mesitylene by ultrasonication and adding 200 μL of 2-allyl-4,4,5,5-tetramethyl-1,3,2-dioxaborolane. The mixture was stirred for 2.5 hours at 120°C under Ar (g) in a Schlenk flask. The particles were recovered by centrifuge, rinsed with toluene and annealed in a 2 mL porcelain combustion boat (VWR, Sugar Land, TX) at 900-950°C for 1 min. This final anneal was under ambient Ar (g) in a quartz tube furnace.

2.2 Optical Microscopy

In preparation for optical studies, the samples were first dispersed in high purity ethanol and sonicated. Drops of suspended VO_2 particles were placed on a glass coverslip and the ethanol allowed to evaporate, leaving behind only the particles that are loosely adhered to the substrate through secondary bonding that results in negligible strain. To further distribute the particles, another coverslip was passed over the surface of the sample to mechanically move, and breakup clumps of particles.

Optical microscopy was performed with an Olympus BX-53 polarized light microscope and images captures by the Olympus UC30 color CCD camera. Images were collected under bright-field-reflected un-polarized white light. Under these conditions a blue shift in the reflected light is observable as the VO_2 particles transition from the low temperature phase M1 to R due to the 600-800 nm decrease in reflectivity in the R phase. Exposure was manually selected and sustained throughout the image series. A Linkham LTS120 Peltier temperature stage with a range of (-25 to 120 °C) with an accuracy of +/- 0.1 °C was used to control the temperature.

2.3 DSC

Differential Scanning Calorimetry (TA Instruments, Q2000) was conducted on ~10 mg of doped and undoped powders at 5 ˚C/min to verify a transformation occurs and to determine the temperature range of the transition of the powder sample. DSC measurement are calibrated using an indium enthalpy standard and has a temperature accuracy of +/- 0.1 ˚C.

CHAPTER 3

RESULTS AND DISCUSSION*

3.1 Phase Equilibria in doped VO_2 Systems

3.1.1 Structural Characterization

The use of X-ray diffraction (XRD) and DSC to evaluate the M1/R phase structures and equilibria (Fig. 2) found that samples incorporating W or B dopants had noticeably depressed equilibrium transformation temperatures. For undoped VO_2 at room temperature, it was expected and confirmed by XRD characterization that the sample would be predominantly in its M1 phase (Fig. 2a). It has been seen in previous studies that the slight broadening of specific reflections in the XRD patterns of W doped VO_2 suggest changes in lattice spacing[19] due to the W dopant causing anisotropic lattice expansion in the M1 phase. This agrees with additional studies conducted that utilize XAFS to determine anisotropic strain[36]. A decrease in phase transition temperatures accompany these structural distortions and therefore, only samples with low dopant concentrations are found predominantly in the monoclinic phase at room temperatures (Fig 2a.). By comparison, the smaller B dopants in interstitial lattice sites cause minimal changes in the lattice parameters[34] and both M1 and R reflections are realized at room temperature due to phase coexistence (Fig 2). Impurity phases, including V_6O_{13} and V_8O_{15}, are identified in small amounts in the undoped and B-doped samples respectively. These impurities are mostly likely caused by aging in atmosphere in the undoped samples and an increase VO_2 reduction during high temperature annealing in

the latter. While these compounds do undergo metal-insulator transitions, their transition temperatures (423 ºC [40] for V_6O_{13} and at -203°C [16] for V_8O_{15}) are far beyond the range sampled here. And therefore, their impacts on these results are minimal.

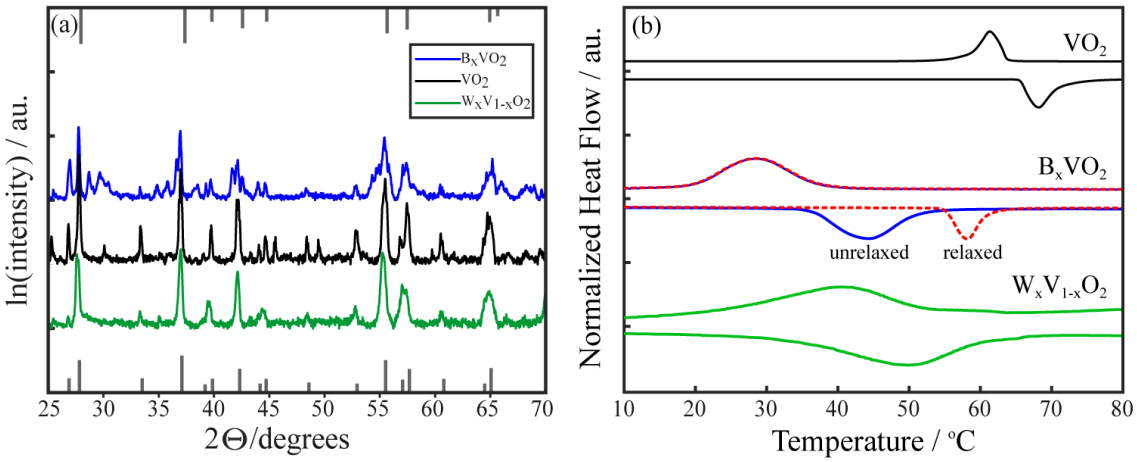

Figure 2: (a) XRD patterns of undoped (black), $B_{0.017}$ VO_2 (blue), and $W_{0.007}V_{0.993}O_2$ (green) samples. Reflections corresponding to the M1 phase of VO_2 are plotted on the lower horizontal axis, whereas reflections corresponding to the R phase of VO_2 are plotted on the upper axis. (b) Normalized DSC traces with a ramp rate of 5 ºC/min are given for undoped (black), $W_{0.0035}V_{0.9965}O_2$ (green), and for a $B_{0.021}VO_2$ sample which was relaxed for a period of 323 days (red) at room temperature as compared with an unrelaxed cycle (blue) of the same sample. This relaxation effect is discussed further below. Reprinted with permission from The Journal of Physical Chemistry C 2020 124 (30),21223-21231

3.1.2 Bulk Transformation Behavior

Depressed transition temperatures and broadened transformation peaks are both observed through DSC characterization with the incorporations of W and B dopants. Peak maxima of DSC traces were taken as critical transition temperatures, and both heating (T_h^{pk} ~68 °C) and cooling (T_c^{pk} ~62 °C) values obtained in undoped samples align with widely accepted transition values [9]. Integrated peak enthalpy (57.7 J/g) is comparable to that reported by *Cook et al.* (52.45 J/g) [17], confirming phase purity and expected transformation behavior in undoped wire VO_2 samples (Fig. 2b). Transition temperatures as measured by DSC were correlated with concentrations determined by XPS and ICP-OES for the specific materials used in this study[34, 41]. Both B and W dopants display a nearly linear relationship between dopant concentration and transition temperature with -10-15 C/atom % and -48-56 C/atom % respectively[34]. Other sample morphologies do display different relationships: W-doped thin films show -10-27.8 C/ atom % while nanobeams contain -18.4 C/ atom % [42, 43]. In addition, theoretical studies of both dopant systems predict slightly different relationships of -18.6-27 C/ atom % of W and 79-83 C/atom % of B [37, 44]. While the overall magnitudes of these relationships differentiate, they are all still decreasing nearly linearly.

Four separate $W_x VO_2$ samples were utilized in this study, with $0.0003 < x < 0.0035$, based on the calibration of T_c^{pk} with W dopant concentration measured by ICP-OES (52 °C/at. % W)[41]. Broad peaks with a maximum width of 30 °C were observed within individual $W_xV_{1-x}O_2$, which indicates either a wide variation of incorporated dopant concentration between particles or a wide span of phase transition within the individual

particles. Only a single nominal concentration of B-doped samples was utilized, $B_{0.017}VO_2$, calculated using the calibration (15 ^{o}C T_c^{pk}/at. %, and T_c^{pk} = 35.46 ^{o}C) as measured by XPS [34]. Similar to the case of W doping, B dopant concentration led to comparatively broad peaks upon heating and cooling (35 ^{o}C), again indicating a range of dopant incorporation or larger degrees of phase coexistence in individual particles. Imaging studies on single nanoparticles described below are capable of differentiating between these two possible origins of the broadened DSC peaks. It must be noted that in B doped samples, cycling and time dependent effects were observed. A B doped particle that has not previously been switched (relaxed) behaves differently through its phase transitions than one that has recently undergone a phase change (unrelaxed). Therefore, this state of being relaxed or unrelaxed is essential for understanding the behavior.

Additionally, W and B dopants introduced varying degrees of peak transformation temperature dependence on DSC scan rate, which contributes to hysteresis measured at fast ramp-rates (> 1 ^{o}C/min). In undoped VO_2, both the peak temperature on cooling (T_c^{pk}) and the peak temperature on heating (T_h^{pk}) symmetrically increased as a function of increasing scan rate. Kinetic dependence of this kind has previously been explained by the Arrhenian nature of rate limiting nucleation barriers between the M1 and R phases[23]. With an increasing ramp rate, there is less time permitted for the high energy nucleation points to be activated and therefor, they trigger at larger degrees of supercooling/ superheating[19]. However, in the case of W-doped samples, no significant dependence on ramp rate for T_c^{pk} or T_h^{pk} is seen. This independence is likely caused by different, more potent nucleation points being utilized[19].

Ramp rate dependence of B-doped VO_2 transition temperatures behaves differently from both undoped and W-doped effects. After a relaxation period of 2 weeks to ensure all particles were fully relaxed following their synthesis, an increase of 12 ^{o}C in heating transition temperature ($T_{\mathrm{h}}^{\mathrm{pk}}$) was observed in a $B_{0.02}VO_2$ sample (near the x = 0.017 concentration observed in this study), and no change in the cooling transition temperature was seen (Fig. 2b). Furthermore, the width of the heating transformation peak experienced a significant reduction peak (24 ^{o}C to12 ^{o}C) with increased relaxation time. This reduction indicated a narrowing of the distribution equilibria transformation temperatures within or between individual particles. Therefore, thermal profiles allowing longer periods of time spent below the heating transition temperature (M1 to R) showed both an increase in $T_{\mathrm{h}}^{\mathrm{pk}}$ and a narrowing of transformation peak. It should be noted that the DSC trace on unrelaxed particles shows similar broad transition peaks and depressed transformation temperatures as seen in *Braham et al*[19].

Independent of ramp rate, hysteresis (measured from peak to peak $\Delta T_{\mathrm{hyst}} = T_{\mathrm{h}}^{\mathrm{pk}} - T_{\mathrm{c}}^{\mathrm{pk}}$) is strongly impacted by the addition of W and B dopants when compared to that of undoped VO_2. ΔT_{hyst} is approximately 5 – 8 ^{o}C for undoped VO_2 (measured at 5 ^{o}C/min in all cases) but varies between 9.3 ± 0.3 to 3.0 ± 0.2^{o}C for $W_xV_{1-x}O_2$ samples as a function of increasing W dopant concentration. Such a scaling has been previously observed and suggested to arise from an increased amount of tensile lattice strain leading to increased degrees of phase coexistence as a function of dopant concentration [45], the individual particle basis of which is further explored in this work. In the limited range of B dopant concentrations studied here, the 'unrelaxed' ΔT_{hyst} is

independent of boron concentration and a uniformly greater magnitude hysteresis is observed compared with undoped samples, ~ 14 ^{o}C.

3.2 Phase Coexistence and Characteristic Domain Size

3.2.1 Undoped VO_2 particles

When undoped VO_2 undergoes its MIT at around ~ 68 ^{o}C, optical microscopy of the distribution of M1 and R phases shows that the phase transition in a large group of individual VO_2 wires (N = 347) occurs abruptly through the particle volume. The MIT occurs at a range of temperatures between the individual particles (Fig. 3, Fig, 4), which indicates nucleation-limited transformation behavior. In this case, phase coexistence is only observed in ~4% or particles. It is likely that within these particles, the phase front is being pinned by a microscopic defect, occurring in a maximum of two temperature increments. Within these two degrees, all of the particles transform completely. By utilizing the intensity of reflected red light as an indicator of existing phase in a designated area, it is possible to extract hysteresis loops corresponding to the extent of transformation (Fig. 3). Within these loops, $T_c^{0.25}$, $T_c^{0.5}$, $T_c^{0.75}$ are defined as the temperature associated with 0.25, 0.5, and 0.75 volume fraction of transformation in the individual particles on cooling, respectively, and $T_h^{0.25}$, $T_h^{0.5}$, $T_h^{0.75}$ represent the same for the case of heating. $T_c^{0.25}$, therefore, signifies the 'start' of the transformation on cooling, while $T_c^{0.t5}$ indicates the transformation's 'end'. From this optical microscopy process, hysteresis loops, calculated transformation width on cooling, ΔT_c, and heating, ΔT_h, (where $\Delta T_c = |T_c^{0.75} - T_c^{0.25}|$) can all be extracted and show that within individual undoped particles, the transformation behavior is symmetric and sharp upon heating and

cooling (Fig. 4). This nucleation limited, symmetric behavior mirrors the phase transition behavior seen in similar free-standing, undoped VO_2 particles that has been widely reported in other studies [21, 46-48].

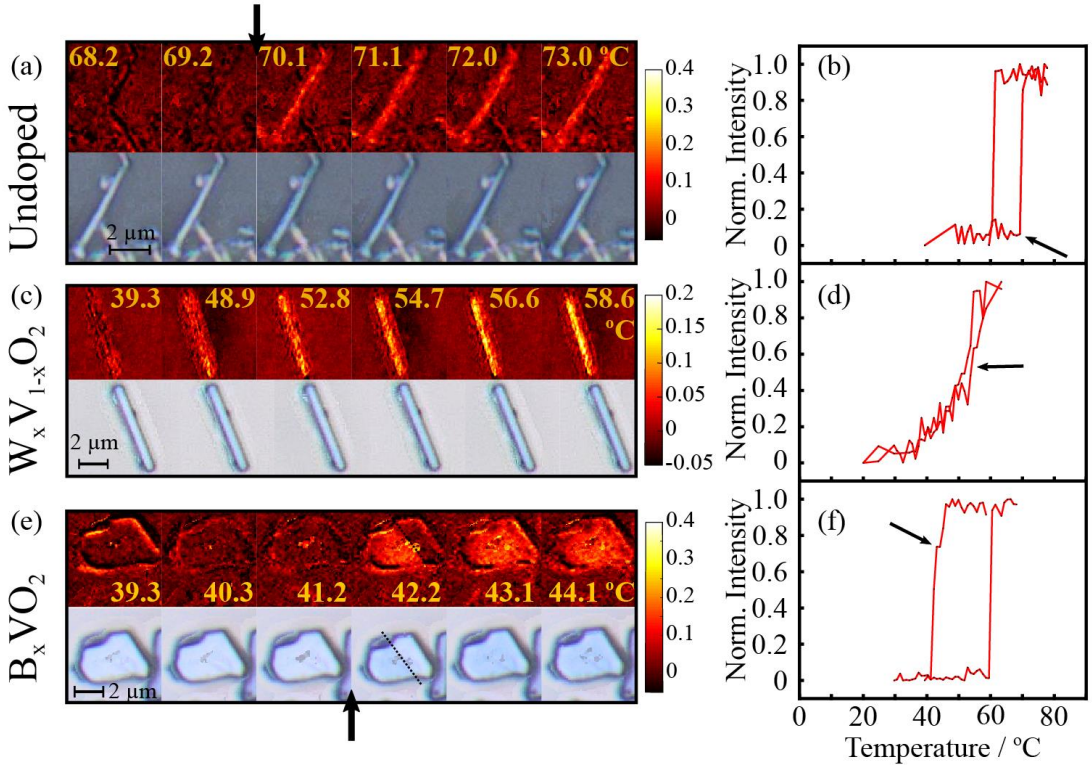

Figure 3: Optical bright-field reflected unpolarized white light images of individual particles, accompanied by extracted cumulative differences in red intensity between base image and images as a function of temperature, for (a) an undoped particle, (c) a $W_xV_{1-x}O_2$ particle, and (e) a B_xVO_2 particle. Normalized cumulative difference for area sums of red pixel intensity for outlined particles between a reference image taken at a base temperature and images at increasing temperature (1 °C increments) are used to track the phase fraction transformed for representative (b) undoped particles (d) $W_xV_{1-x}O_2$ particles showing a variety of transition width symmetries, and (f) B_xVO_2 particles. The black arrows in (a) and (e) indicate the temperature step over which the phase

transforms. Reprinted with permission from The Journal of Physical Chemistry C 2020 124 (30),21223-21231

3.2.2 $W_xV_{1-x}O_2$ Particles

While phase transformation behavior in undoped VO_2 can be categorized as symmetric and abrupt, the transformation in W-doped particles asymmetric and gradual. Most particles of W-doped VO_2 show an extended transformation over multiple temperature intervals without optically distinct domains. Abrupt, clear transitions with characteristic domains on the order of a few microns, most similar to the behavior of undoped VO_2, is only observed in ~0.1% of the particles imaged. Despite the differences in behavior, the phase transition in W-doped particles has comparable changes in red intensity (between 15 and 90 ^oC) to that of undoped VO_2 (Fig. 2), which is nevertheless distinct in reflected unpolarized white light. Due to the gradual nature of the transformation, distinct start and end temperatures are difficult to define. $T_c^{0.25}$, $T_c^{0.5}$ and $T_c^{0.75}$ are calculated from hysteresis loops for individual particles by isolating the specific area associated with a single particle. The progression of the phase transformation can then be evaluated by monitoring the integrated intensity of reflected light (Fig. 3). Despite the inability to optically discern clear domains of the low temperature M1 phase and high temperature R phase, the gradational transition is consistent with characteristic domain length scales in sub-micron regimes, too small to be discerned by optical microscopy. This is corroborated by a study utilizing high-resolution TEM observations of W-doped hydrothermal VO_2 particles which illustrate

phase coexistence on length scales < 10 nm [27]. Additional TEM observations suggest the of M2 phases at the interface between M1 and R phases, another feature not observable at optical length scales [27].

The establishment of a distribution of local equilibria between nanoscale M1, R and M2 domains is considered to be caused by inhomogeneous strain fields around W dopants[19]. In addition to TEM evidence of M1, R and M2 domains, there are several other considerations to support his picture. When observed through XRD, samples with bulk W-dopant concentrations great than 0.5 at. % [19] are seen to have shifted reflections to lower 2θ values and broadened peaks. Both these finding indicate that the W atoms do introduce some anisotropic expansion of the host lattice. It has been previously shown that due to the larger atomic radius of the W atoms compared to V structurally distorts the monoclinic phase lattice towards a more tetragonal-like symmetry and is accompanied by an increase in the interatomic separation of V-V bonds [36] that serves to alter the electronic band gap and phase equilibria. This lattice strain is not resolved in samples with 0.03 – 0.32 at. % W but could likely lay below the refinement limitations of XRD characterization. Samples with the highest W concentration considered in this study (0.32 at. %) would correspond to a W spacing of ~80 nm, in the same order as the domain length scale, while the lowest concentration (0.07 at. %) would produce a spacing of ~350 nm between W dopants. Despite TEM imaging suggesting a homogeneous distribution of W atoms throughout the sample volume [19, 27], it is not known whether W atoms form defect clusters and it is likely that the subsequent stress-fields are neither uniform nor constant. The pattern of domain would therefore be

distributed through the sample in an irregular patchwork as defined by the Multiphysics coupling of dopant localization with surface stresses and particle dimensions or morphology.

It was found that the majority of particles measured possessed symmetric transformation widths. 35% were characterized by their sharp transitions (ΔT_c, $\Delta T_h < 5$ ^oC) on heating and cooling, and 43% displayed gradual transitions during heating and cooling. However, a significant portion of the particles (22%) had distinguishable asymmetries between the transition widths on heating and cooling cycles. Of this subset, ~65% had a characteristically wide heating transition ($\Delta T_h > 5$ ^oC) with an accompanying sharp transition on cooling ($\Delta T_c < 5$ ^oC; Fig. 3). It is likely that this transformation asymmetry stems from disproportionate nucleation or growth barriers between heating and cooling as would be expected if different defect populations were serving as the potent nucleation sites. Separate nucleating defects has been seen in a study on clamped VO_2 wires[24]. It was demonstrated that point defects served as nucleation points on the cooling transition, while higher energy M1 twin boundaries provide a nucleation site for the M1 to R transition [24]. By extension, *Braham et al* have observed kinetic ramp-rate dependence of T_c^{pk} and a lack of dependence of heating transition temperatures on ramp-rate in bulk transformation of $W_xV_{1-x}O_2$ samples ($0.21 < x < 0.32$ at. %). These data are consistent with nucleation at point defects during cooling, and at M1 twins or M1/M2 phase boundaries on heating [19]. The range in transformation behaviors suggest that in individual particles, different nucleation or growth pathways are at work whether that be due to intrinsic defects, dopants or strain.

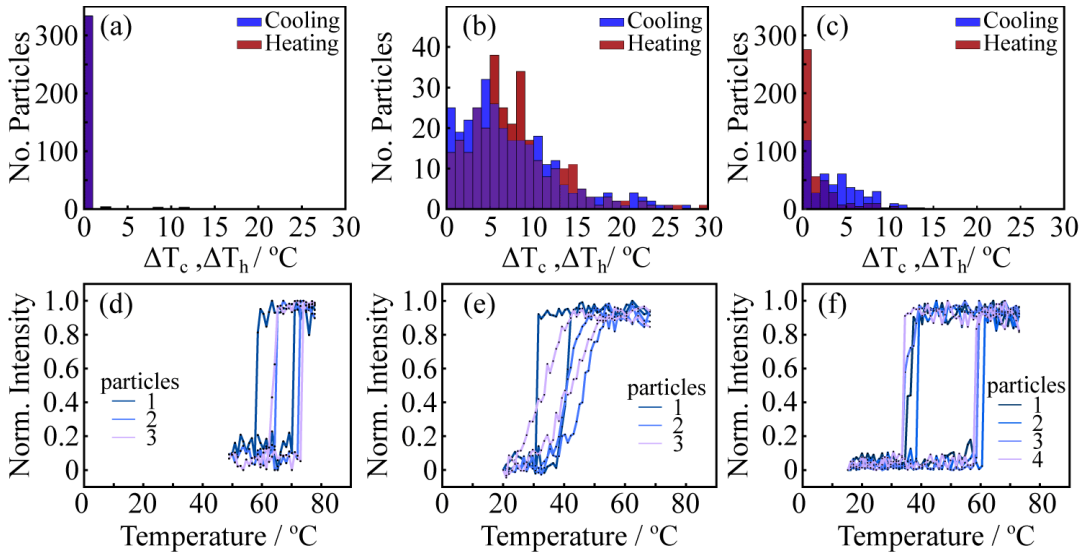

Figure 4: Histograms of the span of heating (red) and cooling (blue) transition widths (ΔT_c, ΔT_h) are given for (a) undoped particles, (b) WxV1-xO2 particles, and (c) BxVO2 particles. Representative hysteresis loops of selected particles for (d) undoped particles, (e) $W_xV_{1-x}O_2$ particles, and (f) B_xVO_2 particles. Reprinted with permission from The Journal of Physical Chemistry C 2020 124 (30),21223-21231

3.2.3 B_xVO_2 Particles

Observations of phase transitions in an ensemble of individual B_xVO_2 particles (N = 399) show that transitions are relatively sharp with clear phase coexistence boundaries discernible at optical length scales. Characteristic domain length scales are on the order of 1.0 ± 0.7 μm^2. Extracted hysteresis loops also show distinct steps over 1 ºC increments on cooling, in stark contrast to the gradual transformations introduced by W dopants (Fig. 3-4). Such micrometer scaling of domain length scales is observed

despite an equivalent dopant concentration as used in W-doped samples, with expected B concentration (1.7 at. %) yielding a spacing of ~10 nm. Such a result is consistent with the small ionic radius of B in an interstitial site which adds minimal distortion to the lattice and the V-V spacing [34]. Therefore, although B is present in high concentrations, inhomogeneous lattice strain gradients are not formed as in the case of W dopant addition, and nanometer scale domains are not stabilized.

The relatively sharp transitions with large extent of phase transition at each step observed in these particles point to a nucleation limited phase transition. For the majority of particles, ΔT_c and ΔT_h both < 1 ^oC. Therefore, DSC observations of wide heating and cooling peaks (~20 ^oC) are associated with chemical equilibria distributed between particles as a result of uneven dopant incorporation, rather than the span of a transition within a single particle (ΔT_c, ΔT_h < 10 ^oC). However, a limited degree of pinning occurs and an asymmetry between heating and cooling transitions is observed in boron-doped particles. For the heating transition, 80% of particles transition with ΔT_h < 1 ^oC. During the cooling transition, only ~30% of particles transition with ΔT_c < 1 ^oC, with a median ΔT_c of 2 ^oC. As in the case of $W_xV_{1-x}O_2$, this asymmetry could stem from differences in nucleation or growth barriers between heating and cooling.

3.3 Effects of Dopants on Transformation Hysteresis

3.3.1 Undoped VO_2 particles

Hysteresis was measured in individual particles as $\Delta T_{\mathrm{hyst}} = T_{\mathrm{h}}^{0.5} - T_{\mathrm{c}}^{0.5}$. Undoped particles demonstrate a wide range of hysteresis from about 5 degrees to more

than 40 (Fig. 5). Most notably, hysteresis in undoped VO_2 is dependent on particle size. $T_h^{0.5}$, $T_c^{0.5}$, and ΔT_{hyst} scale strongly and symmetrically with particle size, with particles < 1 μm^2 experiencing ΔT_{hyst} up to 40 ^oC, and with particles larger than 2 μm^2 having an average ΔT_{hyst} of 8 ^oC (Fig. 6). This observed particle size scaling in hydrothermal VO_2 wires has previously been explained using statistical models developed for observation of nucleation-limited transformation in martensitic Fe-Ni alloy small particle experiments [23, 49-51]. The model assumes defects that serve as potent nucleation sites are sparsely dispersed throughout the volume. Therefore, larger particles contain more potent sites than small particles and are more likely to undergo phase transformation near equilibrium. Because symmetric particle size scaling is observed between heating and cooling transitions, the presence of separate nucleating point defect populations cannot be supported. Fitting of collected transformation data for an ensemble of hydrothermal undoped VO_2 particles to this model resulted in a calculated potent nucleation site density ~ 10^{13} cm^3,[9, 50] which agrees with the qualitative picture of sparse, non-interacting potent nucleation sites.

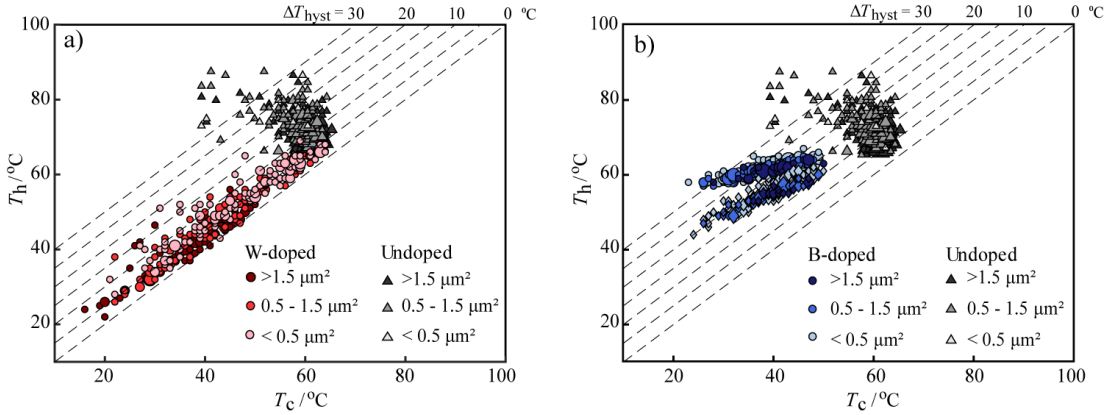

Figure 5: $T_c^{0.5}$ and $T_h^{0.5}$ temperatures of transitions in individual particles demonstrating hysteresis trends binned by particle area for a) W-doped (N = 305) and undoped VO_2 particles (N = 347), and b) B-doped (N=375) and undoped VO_2 particles (N = 347). Iso-hysteresis lines are represented by dashed black lines. Diamonds signify unrelaxed BVO_2 particles and the size of the markers represents how many particles lie at that datapoint. Reprinted with permission from The Journal of Physical Chemistry C 2020 124 (30),21223-21231

3.3.2 $W_xV_{1-x}O_2$ Particles

Introducing W into the VO_2 particles dramatically decreases the transformation hysteresis within a particular particle, while simultaneously increasing the temperature range over which the aggregate transformation occurs (Fig. 5). In 305 individual particles, all were at or below 20 degrees of hysteresis with a few (~1%) showing zero hysteresis (Fig. 5). This is a reduction of the range by more than half that found in undoped VO_2 (45 degrees). Concentration of W-dopant is seen to have no correlation with hysteresis, with highly and lightly doped performing within a few degrees of hysteresis. Additionally, particles that were lightly doped (~0.02 at. %) were able to

retain transformation similar to those seen in undoped VO_2 while maintaining a lower hysteresis (Fig. 5). The broad peaks observed with a maximum width of 30 ^oC measured between peak onset and peak finish in DSC measurements thus derive primarily from inhomogenities in W incorporation across the ensemble of particles as well as an extended phase coexistence regime. However, the observed hysteresis in ensemble measurements relates primarily to variations in W-incorporation across populations of particles.

In comparison to undoped VO_2, hysteresis shows only weak correlation with particle area in $W_xV_{1-x}O_2$ particles ($R = 0.23$, $p = 0.001$, $\alpha = 0.05$; Fig. 4). This lack of scaling of hysteresis in doped VO_2 with particle size is unsurprising in the context of extrinsic doping at high concentrations ~10^{20} cm^3 versus intrinsic potent nucleation site densities ~ 10^{13} cm^3 in undoped VO_2. Similarly, in monoclinic to tetragonal phase transitions in HfO_2 and ZrO_2, particle size scaling is suppressed upon the introduction of extrinsic defects, which serve as more potent and more readily available nucleation sites[9, 51, 52]. Therefore, by introducing point defects or W-dopants the size dependence found in undoped VO_2 can be negated and supplanted by a dopant-perturbation-mediated mechanism.

3.3.3 B_xVO_2 Particles

Overall, B_xVO_2 particles show an increased hysteresis when compared to $W_xV_{1-x}O_2$ particles, reaching a maximum of 35 degrees, nearly equivalent to the bulk of undoped VO_2. Only the undoped particles experience a larger hysteresis. As in $W_xV_{1-x}O_2$ the hysteresis is significantly restricted to a range of 20 degrees in the unrelaxed state.

There are two distinct data sets (relaxed and unrelaxed) to consider in the case of B-doped particles. Fully relaxed particles are seen to have a hysteresis comparable to the highest found in the undoped case, ranging from 15 to 35 degrees. Its unrelaxed state shows a slight decrease in hysteresis compared to its fully relaxed state (Fig. 5). This decrease in hysteresis is especially evident in particles with larger dopant concentrations that subsequently transition at lower temperatures. Furthermore, in the fully relaxed particles, hysteresis is more dependent on dopant concentration as evidenced by the comparison in slopes. The smaller slope and nearly flat distribution of the fully relaxed data indicates that the hysteresis increases with increasing dopant concentration. The data for the unrelaxed particle exhibits a larger slope, closer to what is observed in the W-doped system and shows a uniform hysteresis for the full range of dopant concentrations. This behavior could be caused by simply inequal relaxation times and temperatures due to the cyclic nature of the data collection -- particles with lower transformation temperatures had less time to relax than those at high temperatures.

Similar to $W_xV_{1-x}O_2$ particles, there is no correlation between hysteresis and area in B_x VO_2 particles. However, unlike in the W-doped case, overall hysteresis increases when B-dopants are introduced. This is despite the new, high concentration of point defects. As the B-dopants are relatively small, mobile, and reside in interstitial sites, there is no significant lattice strain caused by their inclusion[34]. Neither is there a large degree of phase coexistence observed like in the W case, which suggests there is less pinning of domain boundaries occurring. The increase in hysteresis indicates that either (i) intrinsic nucleation sites (e.g., oxygen vacancies, vacancy clusters, or dislocations)

are scavenged by introduction of B dopants, or (ii) the nucleation energy barriers are increased by B dopant introduction. Therefore, while B and W dopants suppress size effects in hysteresis of VO_2 as expected from the introduction of extrinsic defects, the overall increase in hysteresis observed in B_xVO_2 samples is non-trivial. However, this explanation does not fully answer why the hysteresis range seen in B_x VO_2 particles is as restricted as that of $W_xV_{1-x}O_2$ (~20 degrees). The tightening of hysteresis in $W_xV_{1-x}O_2$ particles is explained by W-dopants inducing potent nucleation sites which is accompanied by an overall lowered hysteresis. Since B-doped particles do not have a reduced hysteresis an alternate mechanism must exist. It is possible that instead of acting as nucleation sites, the B-dopant scavenges particular intrinsic defects, effectively reducing the range of nucleation while maintaining hysteresis comparable to undoped VO_2. The mobile nature of B atoms renders them amenable to transport to defect sites wherein they can alter local distributions of point defects.

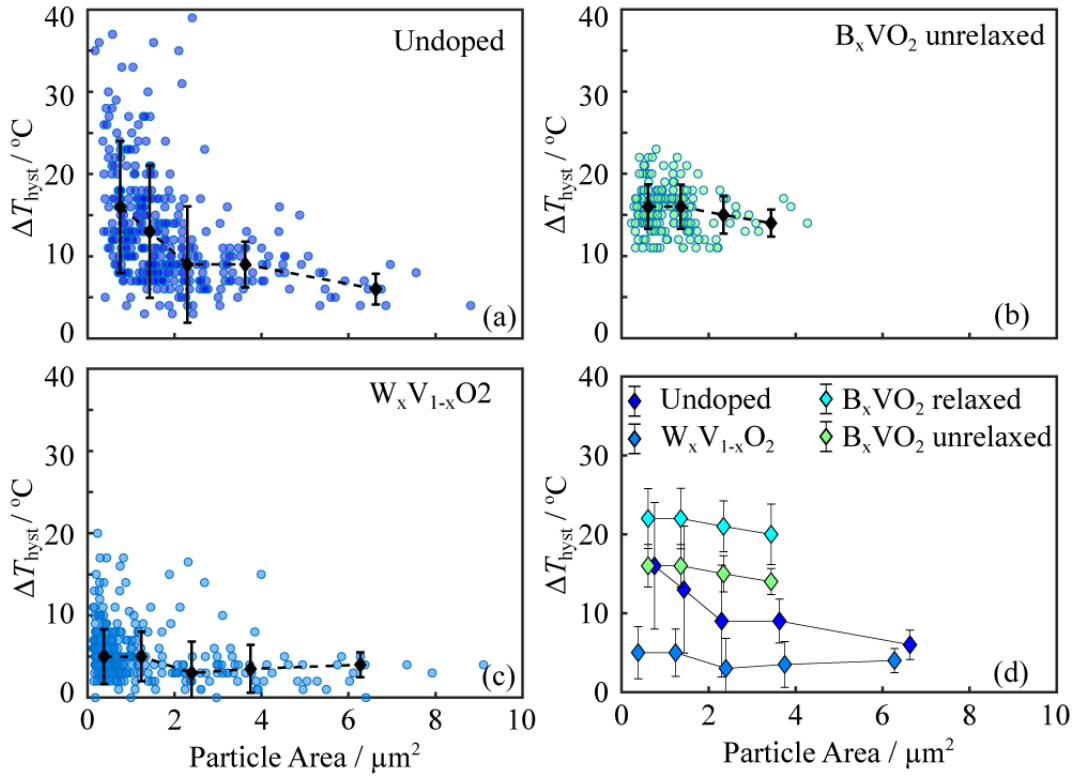

Figure 6: Scaling of hysteresis width as a function of particle area (a) undoped, (b) B_xVO_2, and (c) W_xVO_2 particles. Particle areas are binned with black diamonds to denote their median hysteresis. Reprinted with permission from The Journal of Physical Chemistry C 2020 124 (30),21223-21231

CHAPTER 4

FUTURE WORK

4.1 Ge-Doped

In addition to tungsten and boron doped VO_2 particles, germanium doped samples were also beginning to be analyzed. An ensemble set of N = 332 Ge-doped particles was collected through the optical microscopy technique. These samples were grown utilizing a similar hydrothermal method to that of W-doped particles. The introduction of Ge dopants into the VO_2 system results in behavior quite similar to that of undoped VO_2 and the transitions can largely be categorized as symmetric and abrupt with minimal phase coexistence seen throughout the ensemble of particles. This symmetric transition is centered around the normal, undoped transition temperature of ~ 68 ^oC (Fig. 7a) and accompanied by transition temperatures both on cooling and heating moving towards extremes with increasing dopant concentration along with increasing hysteresis. This behavior is nearly identical to that of the undoped VO_2 (Fig. 7b) with only slightly different slopes.

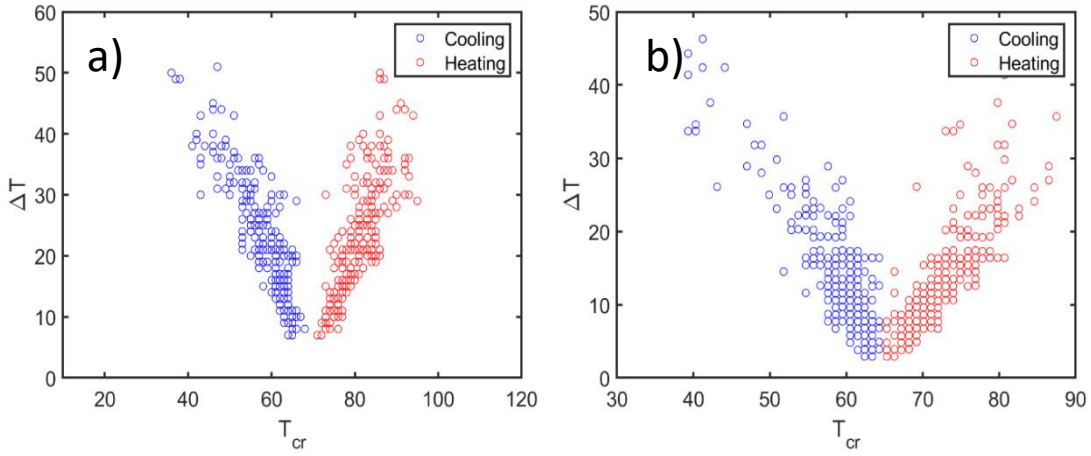

Figure 7: (a) hysteresis plotted against critical temperature Ge-doped VO_2. (b) hysteresis plotted against critical temperature for undoped VO_2.

Ge-doped particles continue to behave similarly to undoped when accounting for its hysteresis behavior is taken into account. This behavior is most obvious when considering Fig X. which plots the transition temperatures on heating and cooling of each individual particle in the undoped and Ge-doped ensembles, resulting in two, largely overlapping clouds. Ge-doped particles, like their undoped counterparts, have a wide range of hysteresis from about 5 degrees to more than 40 (Fig. 8a). However, unlike in undoped, it is difficult to determine if there are any size effects contributing to this wide range of hysteresis due to the limited data on larger particles. Nearly all of the Ge-doped particles were below 0.51 μm^2. When comparing particle area to hysteresis, there is a slight trend that would suggest the influence of size-based effects (Fig. 8b) but further study is necessary to verify this.

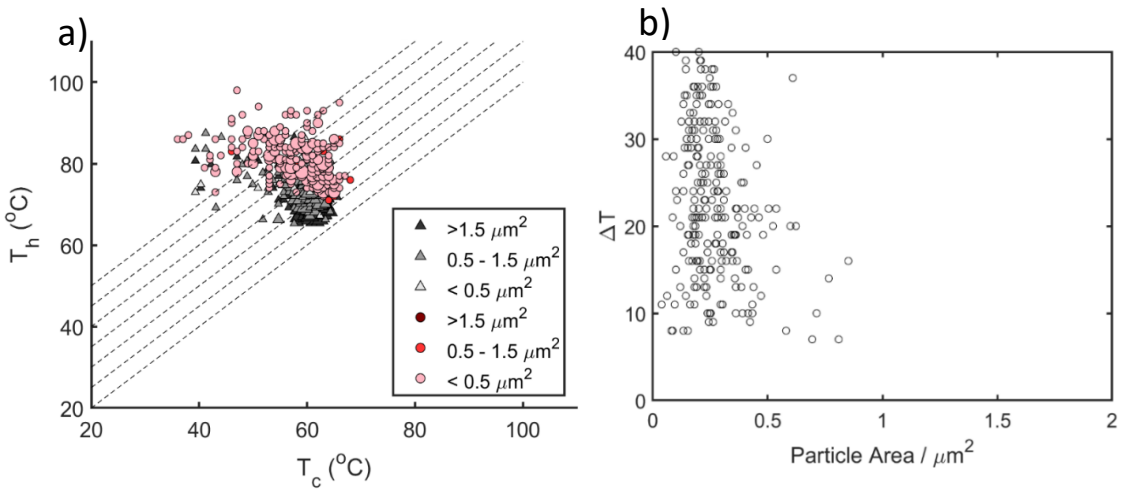

Figure 8: (a) $T_c^{0.5}$ and $T_h^{0.5}$temperatures of transitions in individual particles demonstrating hysteresis trends binned by particle area for a) Ge-doped (N = 332) and undoped VO_2 particles (N = 347). Iso-hysteresis lines are represented by dashed black lines. (b) $T_c^{0.5}$ - $T_h^{0.5}$ =ΔT, hysteresis and particle area of Ge-doped VO_2.

While the analysis on Ge-doped particles has a solid foundation at this point, much work is still to be done to truly understand and draw conclusions. Many of the underlying questions about why the system behaves so analogously to the undoped have yet to be address. Additionally, questions remain about the synthesis process itself. While the data presented here is for hydrothermally grown particles, our chemist collaborators have also succeeded in growing Ge-doped particles through a solid-state process which produces particles that behave vastly different according to their initial DSC characterization. Thorough study of this solid-state germanium system should be conducted before this analysis can be considered completed.

4.2 Irradiation

The entirety of this thesis is focused on the effects of defects in VO_2 transformation behavior. While it has been explored here through different dopants, an alternative method to induce defects is through irradiation. Previous studies into these effects on undoped VO_2 of different morphologies have been conducted. For example, Fan et al investigated the effects of 3 MeV alpha particle irradiation on clamped, undoped VO_2 rods and found that with increasing doses, the transition temperatures converged and hysteresis decreases[24], which is consistent with other comparable studies[24, 53]. However, very few have looked at the combination of irradiation and dopants.

A basic plan to do that has been formulated and the first steps completed. In order to get a close comparison between before and after irradiation while isolating the impact induced defects had on these doped particles, samples for each dopant system (W, B, Ge and undoped) underwent a complete optical analysis and specific particles were identified for the direct comparison. These same particles were used to complete the after-irradiation analysis. These samples were irradiated at low doses in atmosphere and resulted in some issues that need to be addressed to produce clear results. Due to the diminutive size of particles, the fact that they are not bound to the substrate, and changes to the overall morphology of the particles during irradiation, it was difficult to map back to the exact particles imaged in the before-irradiation data. While this issue could be circumvented by looking at large ensemble data sets and trends instead, or simply by being more rigorous with the mapping process, others require tweaks to the

irradiation process. For example, there was significant oxidation or contamination of the samples, which is evident by a yellowing of nearly every sample (Fig 9a). Despite the discoloration effect, most samples were still able to produce distinct color changes over the phase transition. The undoped samples, however, were not transitioning after irradiation and seemed to have fused together into much larger clumps (Fig. 9b), making distinguishing individual particles impossible. It is difficult to tell if this fusion was due to elevated temperatures on the substrates during irradiation or an alternative effect.

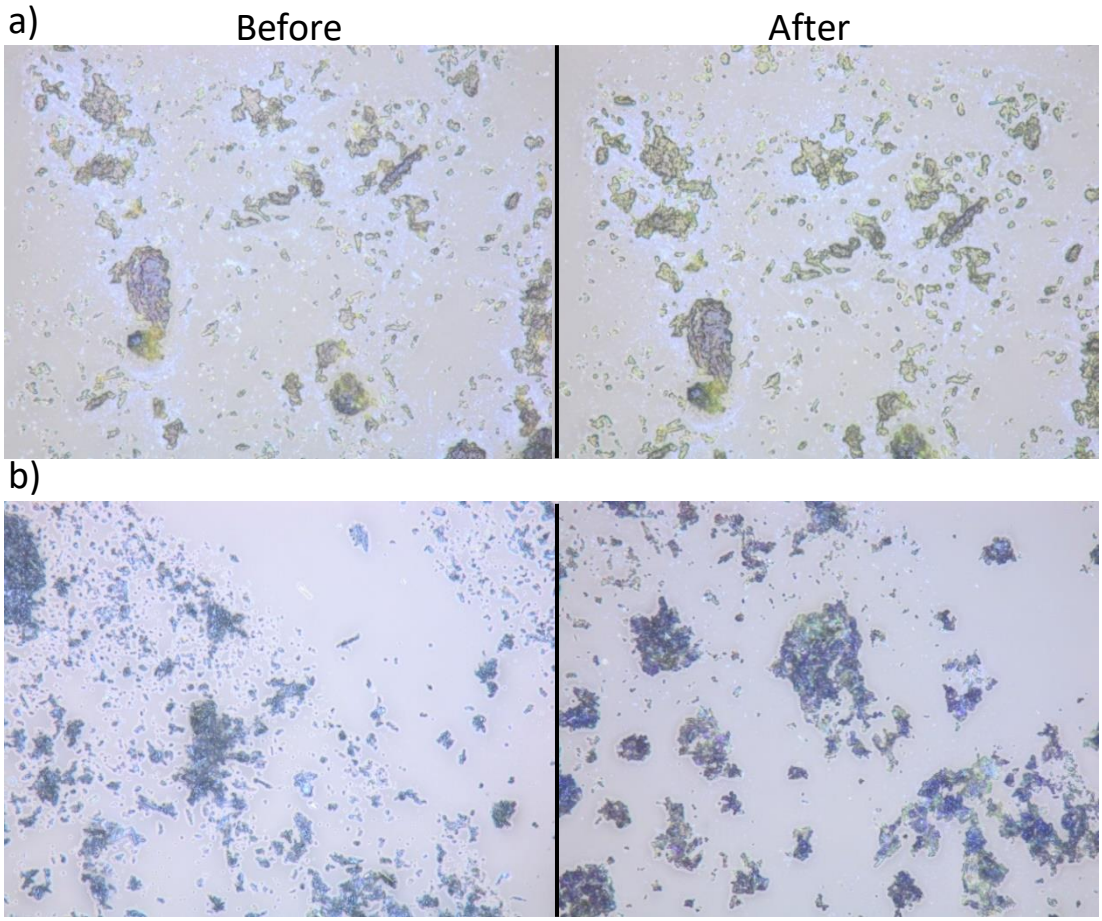

Figure 9: (a) Ge-doped VO_2 (b) Undoped VO_2 images at 100x, taken before and after irradiation exposure.

Despite the difficulties, some data on tungsten, boron and germanium doped systems was produced. Surprisingly, little to no changes were observed when comparing the before and after data for the W-doped and Ge-doped samples (Fig. 10a-b). There was a slight shift observed in the B-doped samples where an increase in transition temperature on heating and cooling can be seen (Fig. 10c). Its possible that due to its

interstitial nature, being smaller and more mobile, the boron doped sample was more susceptible to the irradiation, however, it's hard to draw any conclusions from such a limited dataset. More study is required to give any definitive answers and the experiment process must be refined in order to produce reliable results.

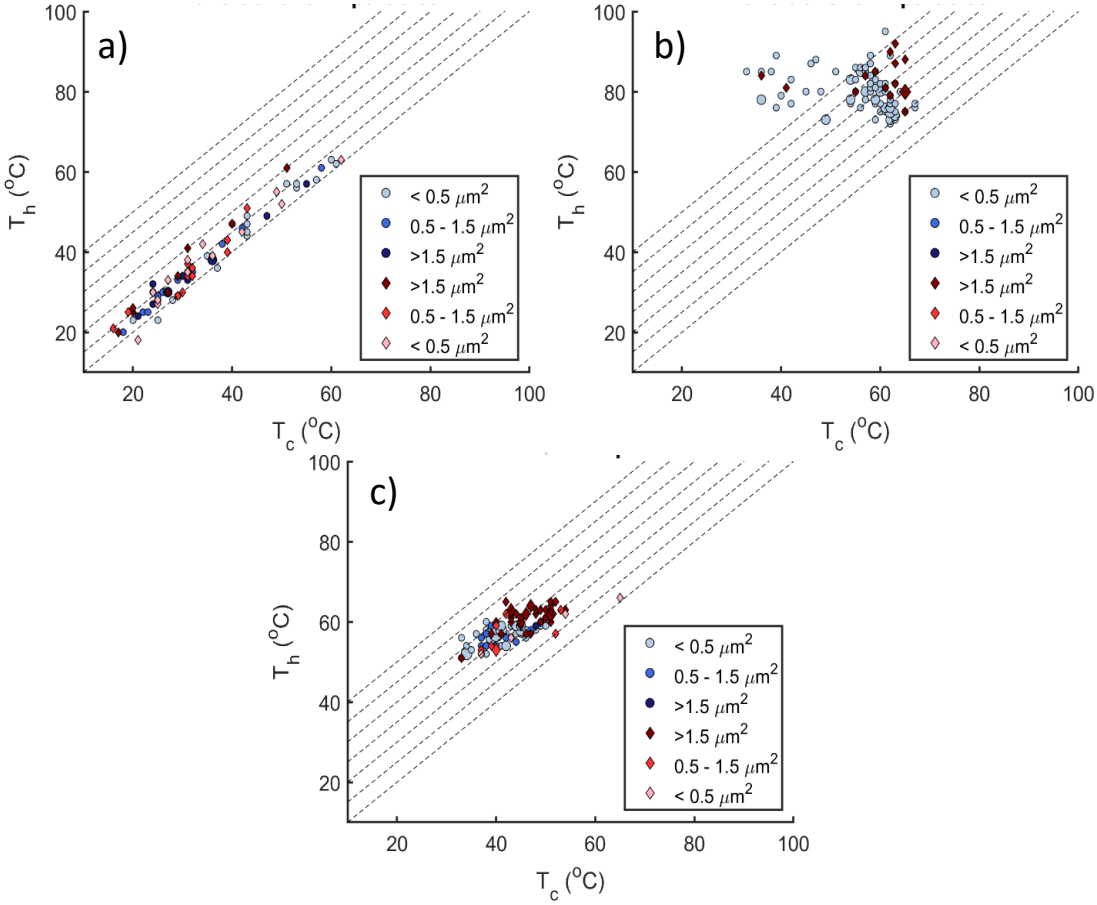

Figure 10: (a) W-doped, (b) Ge-doped, (c) B-doped $T_c^{0.5}$ and $T_h^{0.5}$ temperatures of transitions in individual particles demonstrating hysteresis trends binned by particle area. Blue circle sets indicate before-irradiation data while red diamond sets are after-irradiation.

CHAPTER 5

CONCLUSION

This work decisively shows that incorporating dopants can produce unique transformation behavior beyond simply modifying the transition temperature. W-doping enables a pinning effect that elongates the width of the transformation while still inducing potent nucleation sites that enable nearly zero hysteresis in the system. Alternatively, B-doping shows much smaller transformation widths, less phase coexistence, and maintains a relatively large hysteresis that is much more consistent than in the undoped case. Significantly, doping seems to also suppress size effects, enabling deterministic and reproducible control of hysteresis within dimensionally confined devices. Each of these findings contribute to the overall understanding of the VO_2 MIT behavior and informs further investigation into dopant effects. Given these observations, the incorporation of multiple dopants as a pathway to engineer particular attributes of the MIT transition remains an intriguing possibility, which will be investigated in future work.

REFERENCES

1. Strawn, G.; Strawn, C., Moore's Law at Fifty. *IT Prof.* **2015,** *17* (6), 69-72.

2. Mack, C., THE MULTIPLE LIVES OF MOORE'S LAW. *IEEE Spectr.* **2015,** *52* (4), 31-37.

3. Moore, G. E., Cramming more components onto integrated circuits (Reprinted from Electronics, pg 114-117, April 19, 1965). *Proc. IEEE* **1998,** *86* (1), 82-85.

4. Pickett, M. D.; Williams, R. S., Phase transitions enable computational universality in neuristor-based cellular automata. *Nanotechnology* **2013,** *24* (38), 7.

5. Yi, W.; Tsang, K. K.; Lam, S. K.; Bai, X. W.; Crowell, J. A.; Flores, E. A., Biological plausibility and stochasticity in scalable VO2 active memristor neurons. *Nat. Commun.* **2018,** *9*, 10.

6. Kumar, S.; Williams, R. S., Separation of current density and electric field domains caused by nonlinear electronic instabilities. *Nat. Commun.* **2018,** *9*, 9.

7. Chua, L., Everything You Wish to Know About Memristors But Are Afraid to Ask. *Radioengineering* **2015,** *24* (2), 319-368.

8. Goodenough, J. B., The two components of the crystallographic transition in VO2. *Journal of Solid State Chemistry* **1971,** *3*, 490-500.

9. Morin, F. J., Oxides which Show a Metal-to-Insulator Transition at the Neel Temperature. **1959,** *3*.

10. Kosuge, K.; Kachi, S., Metal-Insulator Transition in VnO2n-1. **1973,** *270*, 258-270.

11. Takahashi, I.; Hibino, M.; Kudo, T., Thermochromic properties of double-doped VO2 thin films prepared by a wet coating method using polyvanadate-based sols containing W and Mo or W and Ti. *Jpn. J. Appl. Phys. Part 1 - Regul. Pap. Short Notes Rev. Pap.* **2001,** *40* (3A), 1391-1395.

12. Verleur, H. W.; Barker, A. S.; Berglund, C. N., OPTICAL PROPERTIES OF VO2 BETWEEN 0.25 AND 5 EV. *Physical Review* **1968,** *172* (3), 788-&.

13. Lee, S.; Hippalgaonkar, K.; Yang, F.; Hong, J. W.; Ko, C.; Suh, J.; Liu, K.; Wang, K.; Urban, J. J.; Zhang, X.; Dames, C.; Hartnoll, S. A.; Delaire, O.; Wu, J. Q., Anomalously low electronic thermal conductivity in metallic vanadium dioxide. *Science* **2017,** *355* (6323), 371-+.

14. Oh, D. W.; Ko, C.; Ramanathan, S.; Cahill, D. G., Thermal conductivity and dynamic heat capacity across the metal-insulator transition in thin film VO2. *Appl. Phys. Lett.* **2010,** *96* (15), 3.

15. Zhou, Y.; Ramanathan, S., Mott Memory and Neuromorphic Devices. *Proc. IEEE* **2015,** *103* (8), 1289-1310.

16. Okinaka, H.; Kosuge, K.; Kachi, S.; Nagasawa, K.; Bando, Y.; Takada, T., Electrical properties of V8O15 single crystal. *Physics Letters A* **1970,** *33* (6), 370-371.

17. Cook, O. A.; Cook, O. A., High-Temperature Heat Contents of V2O3, V2O4 and V2O5. *Journal of the American Chemical Society* **1947,** *69*, 331-333.

18. Budai, J. D.; Hong, J. W.; Manley, M. E.; Specht, E. D.; Li, C. W.; Tischler, J. Z.; Abernathy, D. L.; Said, A. H.; Leu, B. M.; Boatner, L. A.; McQueeney, R. J.;

Delaire, O., Metallization of vanadium dioxide driven by large phonon entropy. *Nature* **2014,** *515* (7528), 535-+.

19. Braham, E. J.; Sellers, D.; Emmons, E.; Villarreal, R.; Asayesh-Ardakani, H.; Fleer, N. A.; Farley, K. E.; Shahbazian-Yassar, R.; Arròyave, R.; Shamberger, P. J.; Banerjee, S., Modulating the Hysteresis of an Electronic Transition: Launching Alternative Transformation Pathways in the Metal-Insulator Transition of Vanadium(IV) Oxide. *Chemistry of Materials* **2018,** *30*, 214-224.

20. Khan, G.; Ahmad, B., Effect of quantum confinement on thermoelectric properties of vanadium dioxide nanofilms. *Applied Physics A* **2017,** *123*.

21. Wu, J.; Gu, Q.; Guiton, B. S.; De Leon, N. P.; Ouyang, L.; Park, H., Strain-induced self organization of metal-insulator domains in single-crystalline VO 2 nanobeams. *Nano Letters* **2006,** *6*, 2313-2317.

22. Vidas, L.; Gunther, C. M.; Miller, T. A.; Pfau, B.; Perez-Salinas, D.; Martinez, E.; Schneider, M.; Guhrs, E.; Galiani, P.; Valvidares, M.; Marvel, R. E.; Hallman, K. A.; Haglund, R. F.; Eisebitt, S.; Wall, S., Imaging Nanometer Phase Coexistence at Defects During the Insulator-Metal Phase Transformation in VO2 Thin Films by Resonant Soft X-ray Holography. *Nano Letters* **2018,** *18* (6), 3449-3453.

23. Clarke, H.; Carraway, B. D.; Sellers, D. G.; Braham, E. J.; Banerjee, S., Nucleation controlled hysteresis in unstrained hydrothermal VO 2 particles. 1-14.

24. Fan, W.; Cao, J.; Seidel, J.; Gu, Y.; Yim, J. W.; Barrett, C.; Yu, K. M.; Ji, J.; Ramesh, R.; Chen, L. Q.; Wu, J., Large kinetic asymmetry in the metal-insulator

transition nucleated at localized and extended defects. *Physical Review B - Condensed Matter and Materials Physics* **2011,** *83*.

25. Wu, J. Q.; Gu, Q.; Guiton, B. S.; de Leon, N. P.; Lian, O. Y.; Park, H., Strain-induced self organization of metal-insulator domains in single-crystalline VO2 nanobeams. *Nano Letters* **2006,** *6* (10), 2313-2317.

26. J. P. Pouget, H. L., Electron Localization Induced by Uniaxial Stress in Pure VO2. *Physical Review Letters* **1975,** *35*, 873-875.

27. Asayesh-Ardakani, H.; Yao, W.; Nie, A.; Marley, P. M.; Braham, E.; Klie, R. F.; Banerjee, S.; Shahbazian-Yassar, R., Direct evidence of M2 phase during the monoclinic-tetragonal (rutile) phase transition of W-doped VO2 nanowires. *Applied Physics Letters* **2017,** *110* (5), 053107.

28. Wei, J.; Ji, H.; Guo, W.; Nevidomskyy, A. H.; Natelson, D., Hydrogen stabilization of metallic vanadium dioxide in single-crystal nanobeams. **2012,** *7*, 357-362.

29. Chen, L.; Wang, X.; Wan, D.; Cui, Y.; Liu, B.; Shi, S.; Luo, H.; Gao, Y., Energetics, electronic and optical properties of X (X = Si, Ge, Sn, Pb) doped VO2(M) from first-principles calculations. *Journal of Alloys and Compounds* **2017,** *693*, 211-220.

30. Du, J.; Gao, Y.; Luo, H.; Kang, L.; Zhang, Z., Solar Energy Materials & Solar Cells Significant changes in phase-transition hysteresis for Ti-doped VO 2 films prepared by polymer-assisted deposition. *Solar Energy Materials and Solar Cells* **2011,** *95*, 469-475.

31. Beteille, F.; Morineau, R.; Livage, J.; Nagano, M., Switching properties of V1-xTixO2 thin films deposited from alkoxides. *Materials Research Bulletin* **1997,** *32* (8), 1109-1117.

32. Patridge, C. J.; Whittaker, L.; Ravel, B.; Banerjee, S., Elucidating the Influence of Local Structure Perturbations on the Metal-Insulator Transitions of V1-xMoxO2 Nanowires: Mechanistic Insights from an X-ray Absorption Spectroscopy Study. *J. Phys. Chem. C* **2012,** *116* (5), 3728-3736.

33. Shibuya, K.; Kawasaki, M.; Tokura, Y., Metal-insulator transition in epitaxial V1-xWxO2(0 < x < 0.33) thin films. *Appl. Phys. Lett.* **2010,** *96* (2), 3.

34. Alivio, T. E. G.; Sellers, D. G.; Asayesh-Ardakani, H.; Braham, E. J.; Horrocks, G. A.; Pelcher, K. E.; Villareal, R.; Zuin, L.; Shamberger, P. J.; Arróyave, R.; Shahbazian-Yassar, R.; Banerjee, S., Postsynthetic Route for Modifying the Metal-Insulator Transition of VO2by Interstitial Dopant Incorporation. *Chemistry of Materials* **2017,** *29*, 5401-5412.

35. Filinchuk, Y.; Tumanov, N. A.; Ban, V.; Ji, H.; Wei, J.; Swift, M. W.; Nevidomskyy, A. H.; Natelson, D., In Situ Diffraction Study of Catalytic Hydrogenation of VO2: Stable Phases and Origins of Metallicity. *Journal of the American Chemical Society* **2014,** *136* (22), 8100-8109.

36. Booth, J. M.; Casey, P. S., Anisotropic structure deformation in the VO2 metal-insulator transition. *Physical Review Letters* **2009,** *103*.

37. Zhang, J. J.; He, H. Y.; Xie, Y.; Pan, B. C., Boron-tuning transition temperature of vanadium dioxide from rutile to monoclinic phase. *The Journal of Chemical Physics* **2014,** *141* (19), 194707.

38. Sellers, D. G.; Braham, E. J.; Villarreal, R.; Zhang, B.; Parija, A.; Brown, T. D.; Alivio, T. E. G.; Clarke, H.; De Jesus, L. R.; Zuin, L.; Prendergast, D.; Qian, X.; Arroyave, R.; Shamberger, P. J.; Banerjee, S., An Atomic Hourglass and Thermometer Based on Diffusion of a Mobile Dopant in VO2. *Journal of the American Chemical Society* **2020**.

39. Asayesh-Ardakani, H.; Nie, A.; Marley, P. M.; Zhu, Y.; Phillips, P. J.; Singh, S.; Mashayek, F.; Sambandamurthy, G.; Low, K. B.; Klie, R. F.; Banerjee, S.; Odegard, G. M.; Shahbazian-Yassar, R., Atomic Origins of Monoclinic-Tetragonal (Rutile) Phase Transition in Doped VO 2 Nanowires. *Nano Letters* **2015,** *15*, 7179-7188.

40. Dernier, P. D., Structural investigation of the metal-insulator transition in V6O13. *Materials Research Bulletin* **1974,** *9*, 955-963.

41. Wu, T. L.; Whittaker, L.; Banerjee, S.; Sambandamurthy, G., Temperature and voltage driven tunable metal-insulator transition in individual WxV1-xO2nanowires. *Physical Review B - Condensed Matter and Materials Physics* **2011,** *83*.

42. Chae, B. G.; Kim, H. T., Effects of W doping on the metal–insulator transition in vanadium dioxide film. *Physica B: Condensed Matter* **2010,** *405* (2), 663-667.

43. Gu, Q.; Falk, A.; Wu, J. Q.; Lian, O. Y.; Park, H., Current-driven phase oscillation and domain-wall propagation in WxV1-xO2 nanobeams. *Nano Letters* **2007,** *7* (2), 363-366.

44. Zhang, J. J.; He, H. Y.; Xie, Y.; Pan, B. C., Theoretical study on the tungsten-induced reduction of transition temperature and the degradation of optical properties for VO2. *J. Chem. Phys.* **2013,** *138* (11), 6.

45. Wu, T.-L.; Whittaker, L.; Banerjee, S.; Sambandamurthy, G., Temperature and voltage driven tunable metal-insulator transition in individual W x V 1− x O 2 nanowires. *Physical Review B* **2011,** *83* (7), 073101.

46. Jones, A. C.; Berweger, S.; Wei, J.; Cobden, D.; Raschke, M. B., Nano-optical investigations of the metal-insulator phase behavior of individual VO2 microcrystals. *Nano Letters* **2010,** *10*, 1574-1581.

47. Tselev, A.; Luk, I. A.; Ivanov, I. N.; Budai, J. D.; Tischler, J. Z.; Strelcov, E.; Kolmakov, A.; Kalinin, S. V., Symmetry Relationship and Strain-Induced Transitions between Insulating M1 and M2 and Metallic R phases of Vanadium Dioxide. **2010**, 4409-4416.

48. Cao, J.; Gu, Y.; Fan, W.; Chen, L. Q.; Ogletree, D. F.; Chen, K.; Tamura, N.; Kunz, M.; Barrett, C.; Seidel, J.; Wu, J., Extended Mapping and Exploration of the Diagram. **2010**, 2667-2673.

49. Olson, G.; Tsuzaki, K.; Cohen, M., Statistical aspects of martensitic nucleation. *MRS Online Proceedings Library Archive* **1985,** *57*.

50. Clarke, H.; Caraway, B. D.; Sellers, D. G.; Braham, E. J.; Banerjee, S.; Arróyave, R.; Shamberger, P. J., Nucleation-controlled hysteresis in unstrained hydrothermal V O 2 particles. *Physical Review Materials* **2018,** *2* (10), 103402.

51. Chen, I.-W.; Chiao, Y.; Tsuzaki, K., Statistics of martensitic nucleation. *Acta Metallurgica* **1985,** *33* (10), 1847-1859.

52. Chen, I.-W.; Chiao, Y., Theory and experiment of martensitic nucleation in ZrO2 containing ceramics and ferrous alloys. *Acta Metallurgica* **1985,** *33* (10), 1827-1845.

53. Leone, A.; Trione, A. M.; Junga, F., Alteration in electrical and infrared switching properties of vanadium oxides due to proton irradiation. *IEEE Transactions on Nuclear Science* **1990,** *37* (6), 1739-1743.